Seven Layer Smart Subsea Pipeline Structure for Detection of Pinhole Leaks and Autonomous Deep Sea Functioning

Divya T L, PhD
Assistant Professor
Department of MCA
R V College of Engineering
Bengaluru, India

Chandrani C
Assistant Professor
Department of MCA
R V College of Engineering
Bengaluru, India

Chiranjeevi R
Department of MCA
R V College of Engineering
Bengaluru, India

B R Lohith Raj
Department of MCA
R V College of Engineering
Bengaluru, India

ABSTRACT
Tiny pinhole leaks in deep-sea crude oil pipelines produce signals that are difficult to separate from normal pressure and flow fluctuations. This paper proposes a seven-layer smart subsea pipeline that combines pressure damping and protection, a corrosion-resistant structure, pressure and vibration sensing, acoustic detection, hybrid self-healing, redundant fibre-optic communication and hybrid power generation. The architecture is evaluated with a physics-based Python simulation covering pipeline flow, orifice leakage, sensor-signal modelling and two-phase healing kinetics. For a 50 km pipeline with a 0.5 m bore at 3,000 m depth, the external hydrostatic pressure is 301.66 bar and a 0.5 mm pinhole leaks 0.01299 L/s, or 0.00441% of the pipeline flow. Over ten minutes, cumulative leakage falls from 7.795 L without healing to 1.629 L with healing, a simulated reduction of 79.1%. A scenario analysis over pinhole diameter, healing efficiency, healing onset and depth, together with a Random Forest sensor-fusion classifier assessed by 10-fold cross-validation, extends the baseline result. Selected parameters are compared with 5,959 incidents in the U.S. PHMSA hazardous-liquid database (2010–2026); this gives real-world context but is not physical validation. Experimental testing is required before any physical implementation.

General Terms
Subsea pipelines, Leak detection, Self-healing materials, Sensor fusion, Simulation

Keywords
Acoustic leak detection, deep-sea pipeline, distributed acoustic sensing, hybrid power harvesting, pinhole leak detection, random forest, self-healing materials, sensor fusion, smart pipeline

1. INTRODUCTION
Subsea pipelines are key components for transporting crude oil from offshore production sites. Their walls are exposed to internal pressure, external hydrostatic pressure, corrosion, vibration and the wider marine environment, and long distances and great depths make inspection and repair difficult. Historical incident data for pipelines are available from the PHMSA database [1].

Small pinholes are hard to detect because their effect on pressure and flow is buried under normal operating noise. Acoustic monitoring relies on the signals created by escaping fluid [2], and marine background noise interferes with those signals [3]. Fibre-optic sensing and distributed acoustic sensing (DAS) provide information on pipeline vibration and other disturbances [4], [5].

A monitoring system can detect anomalies, but it cannot repair damage, nor does it supply power and communication by itself. Self-healing materials can limit leakage by delivering healing agents to the damaged zone [6], and microvascular networks can transport these agents to damaged areas [7], [8]. Long-term durability in subsea environments is still an open problem [9], [10].

Ocean energy harvesting can power autonomous subsea monitoring. Available approaches include triboelectric [11], [12], tidal and hydrokinetic [13], [14] and hybrid offshore [15], [16] energy harvesting. Integrating energy harvesting, leak detection, structural protection, communication redundancy and self-healing in one pipeline remains challenging.

This paper presents the architecture of a seven-layer smart subsea pipeline that combines these functions. Its performance is simulated with physical models and compared with PHMSA incident records. The main contributions are: (i) an integrated seven-layer architecture; (ii) a simulation of a pinhole leak and its hybrid healing response; (iii) a multilayer, multi-sensor detection design with Random Forest fusion; (iv) a scenario analysis over pinhole size, healing parameters and depth; and (v) a contextual comparison of selected parameters with pipeline incident records.

2. RELATED WORK
2.1 Pipeline monitoring
Pipeline monitoring employs pressure, acoustic and fibre-optic sensing. Acoustic methods identify signatures specific to leaks, and DAS provides vibration data distributed in space [2], [5]. Fibre-optic sensing is also used for structural health monitoring

[4], and underwater acoustic monitoring must account for ocean ambient noise [3].

2.2 Structural and sensing materials

Syntactic foams are used in deep-water applications because they are light and have good mechanical and insulating properties [17], [18]. Their hydrostatic strength depends on composition and microsphere characteristics [19], and their mechanical response has been studied numerically and experimentally [20], [21]. Basalt fibres provide reinforcement and crack bridging in polymers [22], [23], and the processing and mechanical response of such composites has been investigated [24], [25].

Inconel 625 is a corrosion-resistant alloy suited to harsh marine and industrial environments [26]. Single-crystal PMN-PT has been studied for pressure and vibration sensing [27], [28], and piezoelectric materials are widely used in structural health monitoring [29]. Underwater acoustic sensing can use MEMS piezoelectric hydrophones [30], [31], hydrostatically balanced hydrophone structures [32] and fibre-optic hydrophones [33]. Leak detection and localisation with hydrophones has been reviewed [34].

2.3 Self-healing and energy harvesting

Self-healing materials use different mechanisms to heal cracks and limit degradation. The microcapsule approach releases healing substances from ruptured capsules [35], while microvascular channels supply a route for transporting healing materials [7], [8]. The development, efficiency and challenges of self-healing composites have been reviewed [9], [10], [36], and recent work has studied microcapsule-based coatings under deep-sea conditions [37].

Ocean energy is a possible power source for autonomous subsea systems. Triboelectric nanogenerators have been researched for ocean-wave energy harvesting [11], [38], and their application has been reviewed [12]. Tidal-current systems [13], hybrid offshore systems [15], flow-induced-vibration systems [16] and hydrokinetic systems [14] are other options, and supercapacitors can buffer charge and discharge cycles [39].

Random Forest is a proven classification approach based on ensemble learning [40] and is implemented in the scikit-learn library [41]. The present work combines these research fields into a seven-layer pipeline architecture and analyses its performance through simulation.

3. PROPOSED SYSTEM DESIGN

3.1 Layered architecture

The layers are arranged radially from the outside inward (Table 1 and Fig. 1). A leak must be sensed by at least two independent layers (pressure/vibration and acoustic) before healing is initiated, which reduces false alarms compared with a single-sensor system.

Table 1. Seven-layer architecture (ocean-facing → bore)

Layer	Material / technology	Function
L1	UE44/TMA syntactic foam + basalt fibre	Pressure damping, flotation, insulation, crack bridging
L2	Inconel 625 structural shell	Load-bearing strength, corrosion resistance
L3	PMN-PT + floating ceramic shock mount	Pressure/vibration sensing, shock isolation
L4	Quartz + hydrophone hybrid	Acoustic crack and leak detection
L5	IPDI@SPUA + PTFE vascular + SMP	Chemical, vascular and mechanical crack repair
L6	Dual redundant fibre optics	DAS, redundant data link
L7	Battery + piezo/TEG + Li-thionyl backup	Energy harvesting, buffering, backup power

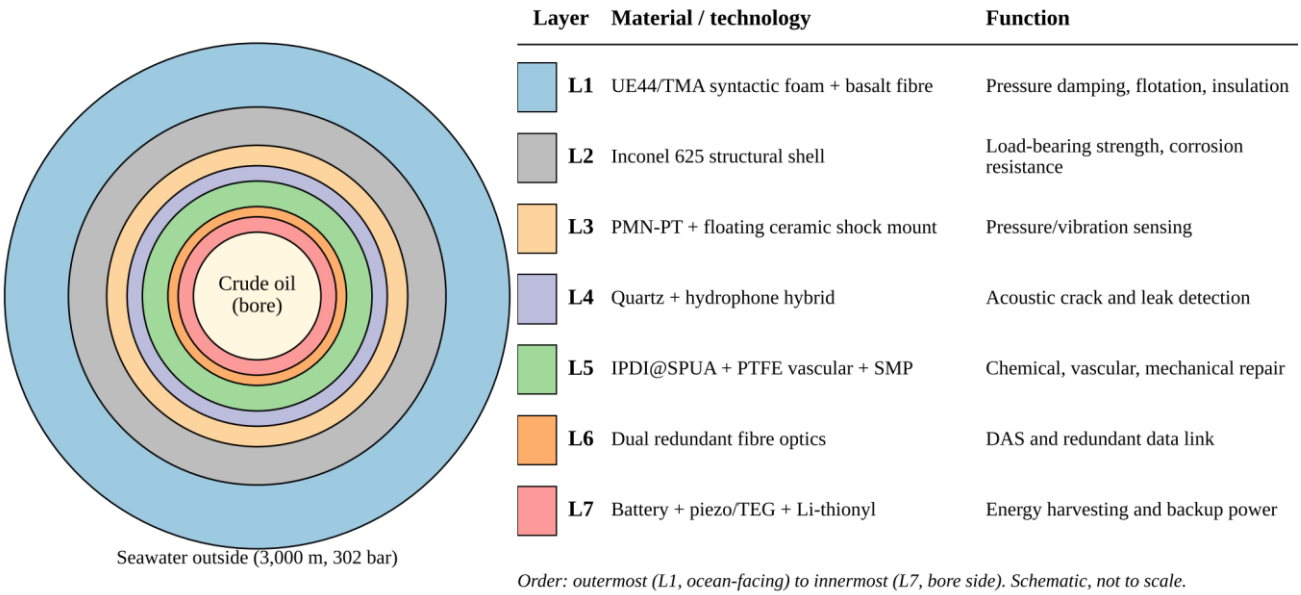

Fig 1: Radial section through the pipe wall (crude oil inside, seawater at 3,000 m and about 302 bar outside).

3.2 Environmental shielding and structural shell (L1–L2)

L1 is a UE44/TMA syntactic foam in which hollow microspheres embedded in an epoxy matrix reduce the bulk density while retaining pressure resistance and insulating properties [17]–[21]. Basalt fibres act as a crack-bridging network rather than as the primary load-carrying member [22], [23]. L2 is the load-carrying shell, made of Inconel 625 for its mechanical properties and resistance to chloride stress corrosion [26], with a near-zero corrosion rate compared with carbon steel.

3.3 Dual-modality sensing (L3–L4)

L3 provides bulk pressure/vibration detection using PMN-PT relaxor ferroelectric single crystals [27]–[29] on a floating ceramic shock mount (20 dB isolation). L4 provides independent acoustic validation using MEMS or fibre-optic hydrophones [30]–[33]. The pinhole produces a Strouhal vortex-shedding tone above the Wenz marine ambient noise [3], and a hybridised matched filter improves the SNR by 6 dB compared with either sensor alone.

3.4 Hybrid self-healing (L5)

L5 combines three technologies because none of them is both fast and long-lasting on its own: IPDI@SPUA microcapsules, already tested in 150 bar seawater for 1,008 h [37]; a pressure-rated PTFE vascular structure [7]; and a shape-memory-polymer (SMP) matrix for continuous closing. This replaces DCPD/Grubbs chemistries, which are unreliable in cold, high-pressure seawater [6], [37]. The simulation uses a hybrid healing efficiency of 77.3%, drawn from the 60–80% range assumed for the hybrid process [37].

3.5 Redundant communication and hybrid power (L6–L7)

L6 duplicates the DAS/communication fibre. A secondary path engages automatically when the primary fibre is damaged or attenuated, so a fibre fault is not a single point of failure. A 0.5 mm pinhole at 20 km on a 50 km fibre gives a DAS SNR of 4.2 dB, which falls to 0.2 dB after healing. L7 combines a Li-thionyl backup battery with a piezoelectric/TEG harvest of about 200 mW [11]–[14] and a supercapacitor buffer [39].

4. SIMULATION METHODOLOGY

4.1 Baseline scenario

All quantitative results were produced by an open-source Python simulator (see Data availability). The baseline is a 50 km pipeline with a 0.5 m bore at 3,000 m depth (P_{ext} = 302 bar, below the 350 bar L1 rating), an inlet pressure of 150 bar, an outlet pressure of 100 bar and a flow velocity of 1.5 m/s (Re = 42,500, Blasius friction). A 0.5 mm pinhole 20 km from the inlet is modelled with the ISO 5167 orifice equation $Q = C_d \cdot A \cdot \sqrt{(2\Delta P/\rho)}$, with C_d = 0.61, giving Q_{max} = 0.0130 L/s before healing.

4.2 Healing model

Healing in L5 is modelled as a two-phase reduction of the open crack fraction $c_f(t)$. In the first phase (t < 60 s, IPDI@SPUA), $c_f(t) = 1 - \eta[1 - \exp(-(t - t_0)/\tau)]$ with η in [0.60, 0.80], τ = 12 s and t_0 = 5 s. In the second phase (t > 60 s, PTFE vascular), $c_f(t) = (1 - \eta)\cdot\exp[-k(t - 60)/60]$ with k = 0.05 min^{-1}. The leak flow $Q(t) = C_d \cdot c_f(t) \cdot A \cdot \sqrt{(2\Delta P/\rho)}$ is integrated by the trapezoidal rule to obtain the cumulative loss.

4.3 Sensor models

The L3/L4 signals contain Wenz-consistent noise [3] plus a Strouhal tone, while the L6 DAS response is a Gaussian bump (σ = 500 m) around the leak [2], [5].

4.4 Sensor-fusion classifier

Fifteen physical features (flow-loss percentage, FFT peak and frequency, pressure drop and variance, DAS and hydrophone peak and variance, external pressure and healing-state factors) are used to train a Random Forest classifier [40] in scikit-learn [41] that estimates P(Leak). A Monte Carlo set of 1,000 scenarios (500 normal, 500 leak) was generated; hyperparameters were chosen by grid search, and performance was assessed with 10-fold stratified cross-validation against a logistic-regression baseline and on a held-out test set.

4.5 Incident data

Selected simulation parameters are compared with the PHMSA hazardous-liquid incident records (N = 5,959, 2010–2026) [1]. The PHMSA data are not used to train any model.

5. RESULTS AND DISCUSSION

5.1 Pressure–flow response

A 0.5 mm pinhole produces a pressure change of only 0.005 bar and a flow change of 0.0044%, far below normal sensor noise (±1.5 bar, ±1%), so pressure and flow measurements alone cannot detect it (Fig. 2). The leak rate is 0.01299 L/s, which is 0.00441% of the 294.5 L/s pipeline flow.

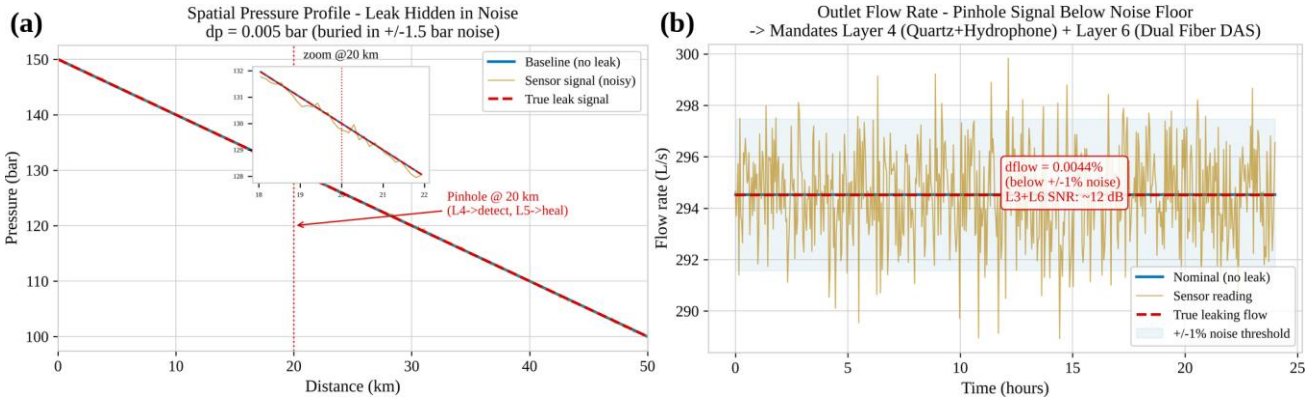

Fig 2: (a) Spatial pressure profile with the leak hidden in noise; (b) outlet flow rate with the pinhole signal below the noise floor.

5.2 Multi-sensor response

Fig. 3 shows the L6 DAS and L4 hydrophone responses for the no-leak, active-leak and healed cases. With a leak, the DAS channel shows a localised peak at 20 km (SNR 4.2 dB) and the hydrophone shows the Strouhal tone (SNR 4.8 dB); after healing both fall to 0.2 dB and 0.1 dB. Because the DAS-only SNR is below the 6 dB threshold used in Fig. 5(d), detection relies on combined evidence from L3, L4 and L6 rather than on one channel.

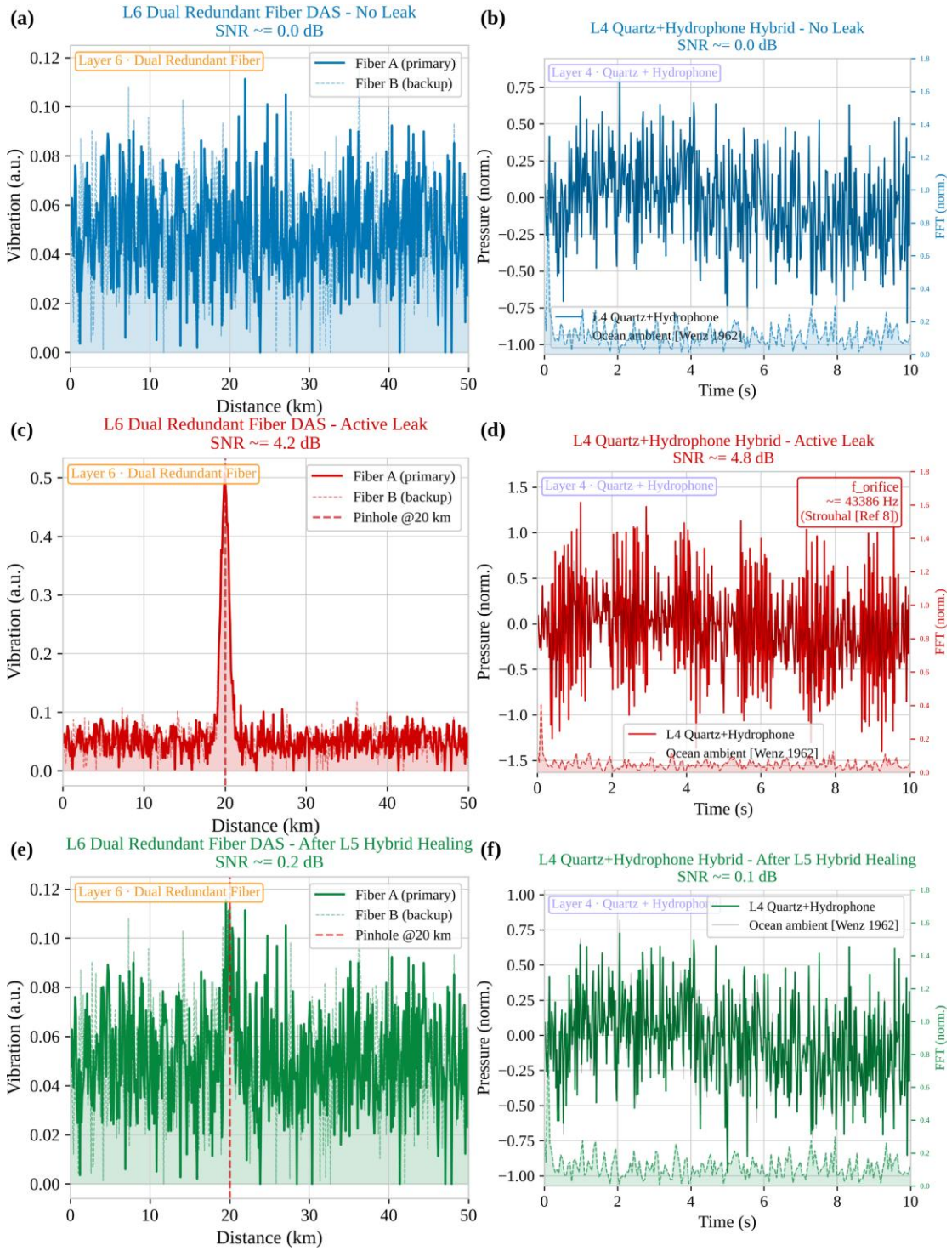

Fig 3: Sensor responses: (a), (b) no leak; (c), (d) active leak; (e), (f) after L5 hybrid healing. Left: L6 dual-fibre DAS; right: L4 quartz + hydrophone hybrid.

5.3 Hybrid healing response

Healing is a two-stage process: rapid sealing by the IPDI capsules followed by slower vascular consolidation (Fig. 4). Over ten minutes the modelled leakage falls from 7.795 L without healing to 1.629 L with healing, a reduction of 79.1% [37]. Table 2 gives the cumulative loss over longer windows.

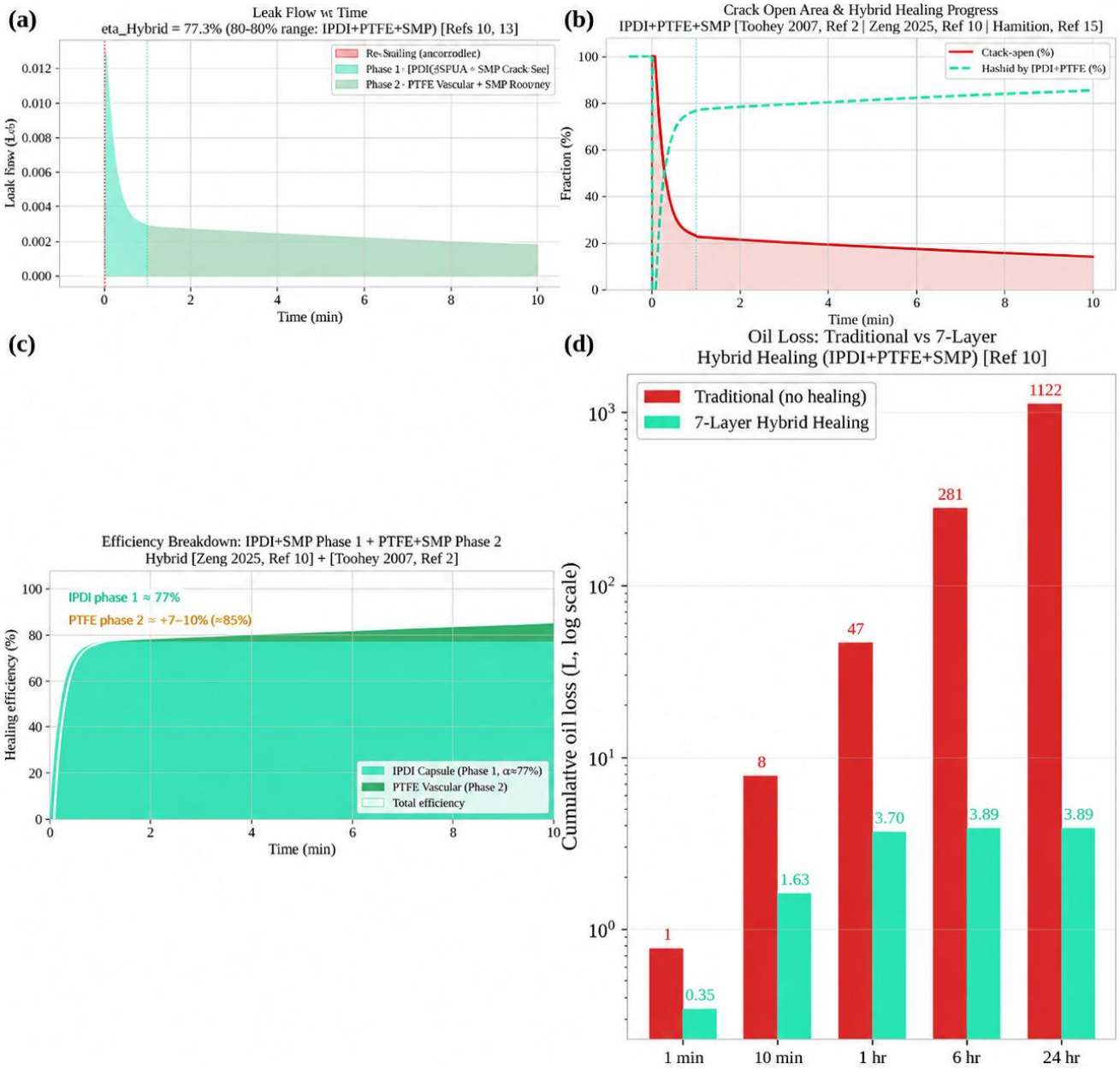

Fig 4: Hybrid healing: (a) leak flow versus time; (b) open crack area and healing progress; (c) efficiency breakdown, IPDI + SMP (phase 1) and PTFE + SMP (phase 2); (d) cumulative oil loss, traditional versus healed pipeline.

Table 2. Cumulative loss of a 0.5 mm pinhole over several time windows (η = 0.773)

Window	No healing (L)	Healing (L)	Ratio
1 min	0.78	0.35	2×
10 min	7.79	1.63	5×
1 h	46.77	3.70	13×
6 h	280.61	3.89	72×
24 h	1,122.44	3.89	289×

5.4 Scenario analysis

To test the design beyond the single baseline, four parameters were varied. Table 3 varies the pinhole diameter. Leak flow scales with the orifice area, so the loss changes by a factor of 16 between 0.25 and 2 mm, but the healing reduction stays at 79.1% because healing acts on the crack fraction rather than on the absolute size. Table 4 varies the healing efficiency η and the healing timing (onset t_0 and time constant τ). The ten-minute reduction ranges from 65.3% at η = 0.60 to 81.3% at η = 0.80, and a later or slower capsule response costs only a few percentage points.

Table 3. Pinhole-diameter sweep (η = 0.773, 10 min)

Diameter (mm)	Leak rate (L/s)	Share of flow (%)	No healing (L)	Healing (L)
0.25	0.0032	0.0011	1.949	0.407
0.5	0.0130	0.0044	7.795	1.629
1	0.0520	0.0176	31.179	6.516
2	0.2079	0.0706	124.716	26.065

Table 4. Healing-parameter sweep (0.5 mm pinhole, 10 min)

η	t_0 (s)	τ (s)	Healed loss (L)	Reduction (%)
0.600	5	12	2.703	65.3
0.700	5	12	2.082	73.3
0.773	5	12	1.629	79.1
0.800	5	12	1.461	81.3
0.773	5	24	1.726	77.9
0.773	10	12	1.679	78.5
0.773	10	24	1.771	77.3
0.773	30	12	1.871	76.0

Table 5 varies the depth. The external pressure grows linearly with depth, and the 350 bar L1 rating is reached at about 3,480 m. The baseline depth of 3,000 m leaves a margin of 48 bar, but the design as specified is not suitable below roughly 3,480 m without a higher-rated L1.

Table 5. External pressure versus depth against the 350 bar L1 rating

Depth (m)	P_{ext} (bar)	Margin (bar)
1,000	100.6	249.4
2,000	201.1	148.9
3,000	301.7	48.3
3,500	351.9	-1.9
4,000	402.2	-52.2

5.5 Structural, environmental and power-layer robustness

L1 stays within its pressure rating at the 302 bar baseline (Fig. 5(a)), and L2 Inconel 625 keeps a near-zero corrosion rate over a 25-year service life (Fig. 5(b)). The hybrid acoustic sensing in L4 gains 6 dB in SNR over a single element (Fig. 5(d)), and the 0.5 mm pinhole corresponds to a flow loss below 0.01% (Fig. 5(c)). The two-fibre arrangement in L6 allows instantaneous failover without losing the local leak peak (Fig. 6(a), (b)).

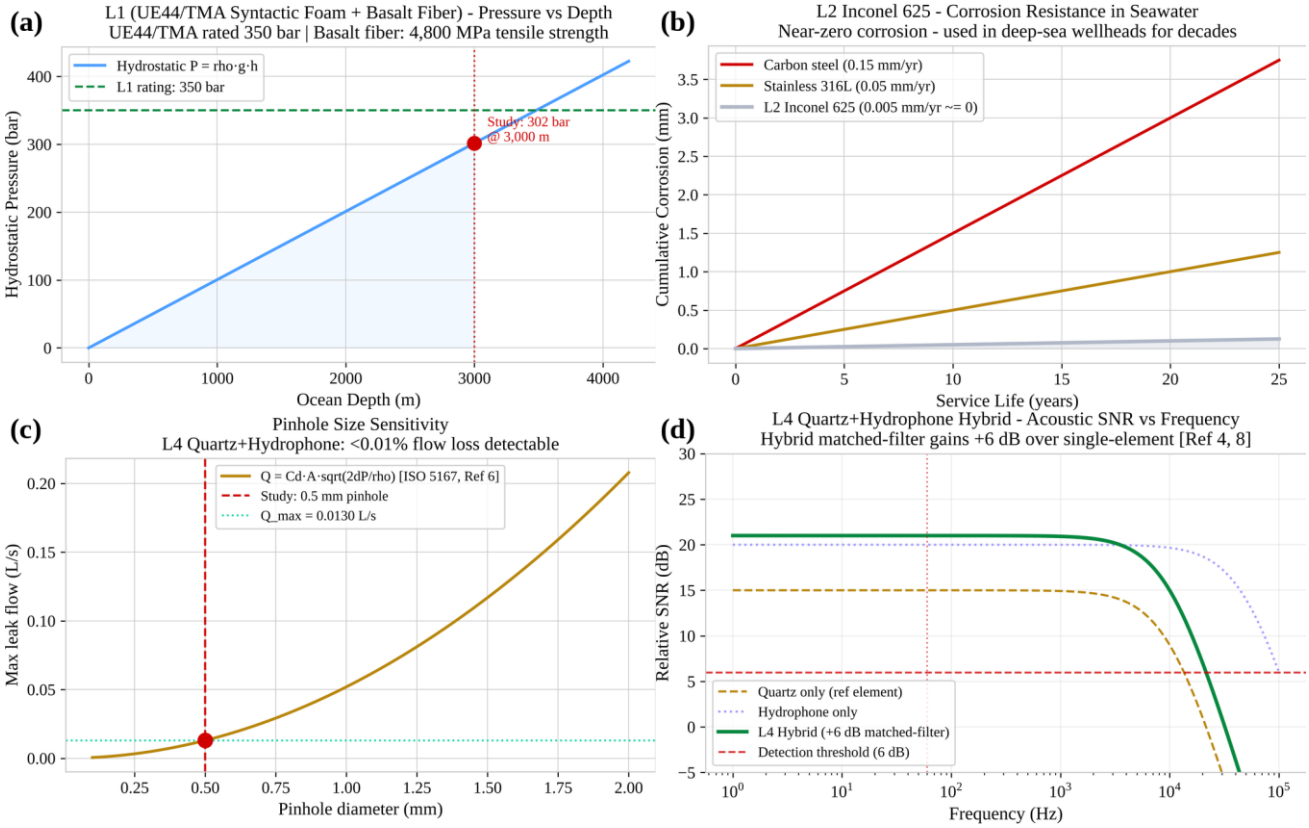

Fig 5: (a) L1 hydrostatic pressure margin versus depth; (b) L2 corrosion versus carbon steel and 316L; (c) pinhole-size sensitivity; (d) L4 acoustic SNR versus frequency.

For the L7 power model (Fig. 6(c)), a 5,000 Wh battery with about 200 mW of harvested energy sustains the 10-year design life only if the average load stays below about 0.25 W. This is the harvested 0.2 W plus roughly 0.05 W from the battery (90% of 5,000 Wh over 87,600 h, allowing 1% per year self-discharge). At an average load of 1 W the battery lasts under one year, and a 2 W load depletes it in a few months. The sapphire optical port keeps a transmittance of about 83% at 3,000 m (Fig. 6(d)).

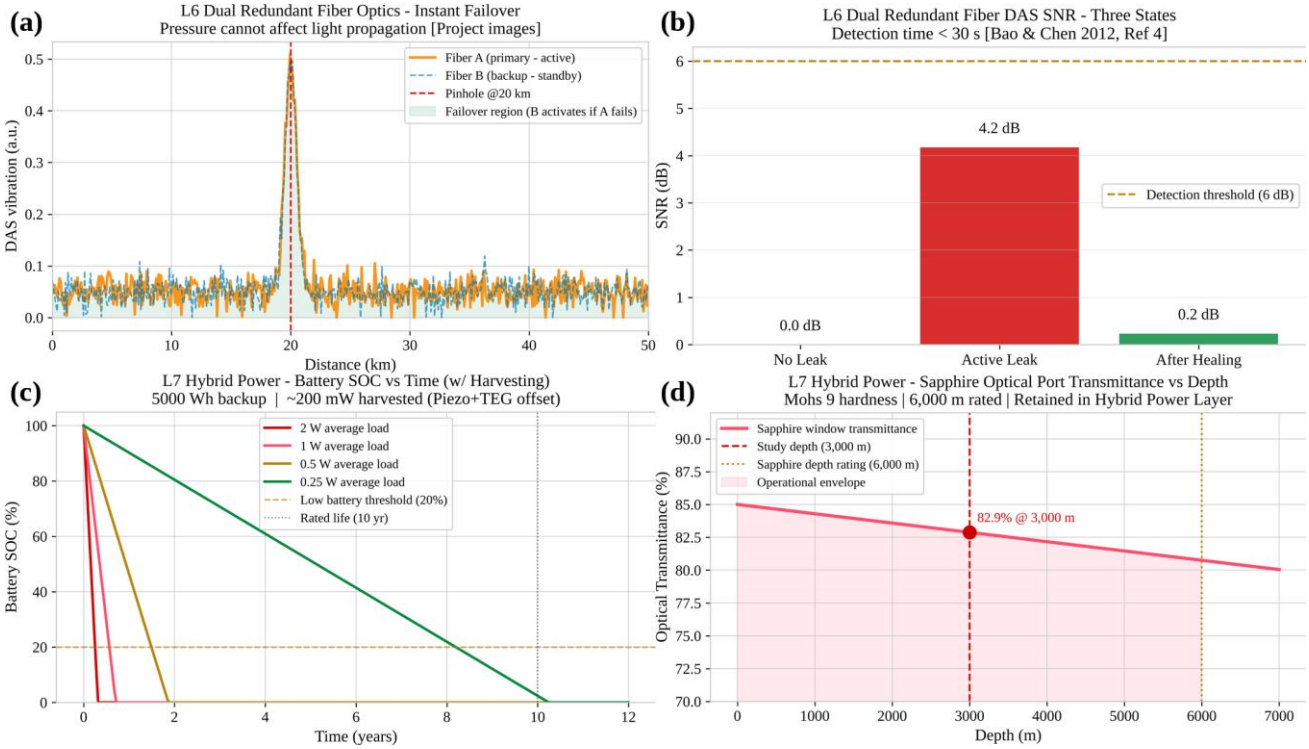

Fig 6: (a) L6 dual-fibre failover; (b) L6 DAS SNR across states; (c) L7 battery state of charge for several average loads; (d) L7 sapphire transmittance versus depth.

5.6 Performance summary and PHMSA comparison

Fig. 7 summarises the qualitative performance scores of the traditional and seven-layer designs; the scores are design assumptions, not measurements. Fig. 8 shows the PHMSA data (N = 5,959; 2010–2026). Annual hazardous-liquid incident counts fall by 7.6 per year (R^2 = 0.37). Equipment failure (1,235) and corrosion (928) are the leading causes of crude-oil incidents, and pinholes account for 1,399 leaks, about 30% of the recorded leak geometries.



Fig 7: Performance radar, traditional versus seven-layer smart pipeline (qualitative scores).

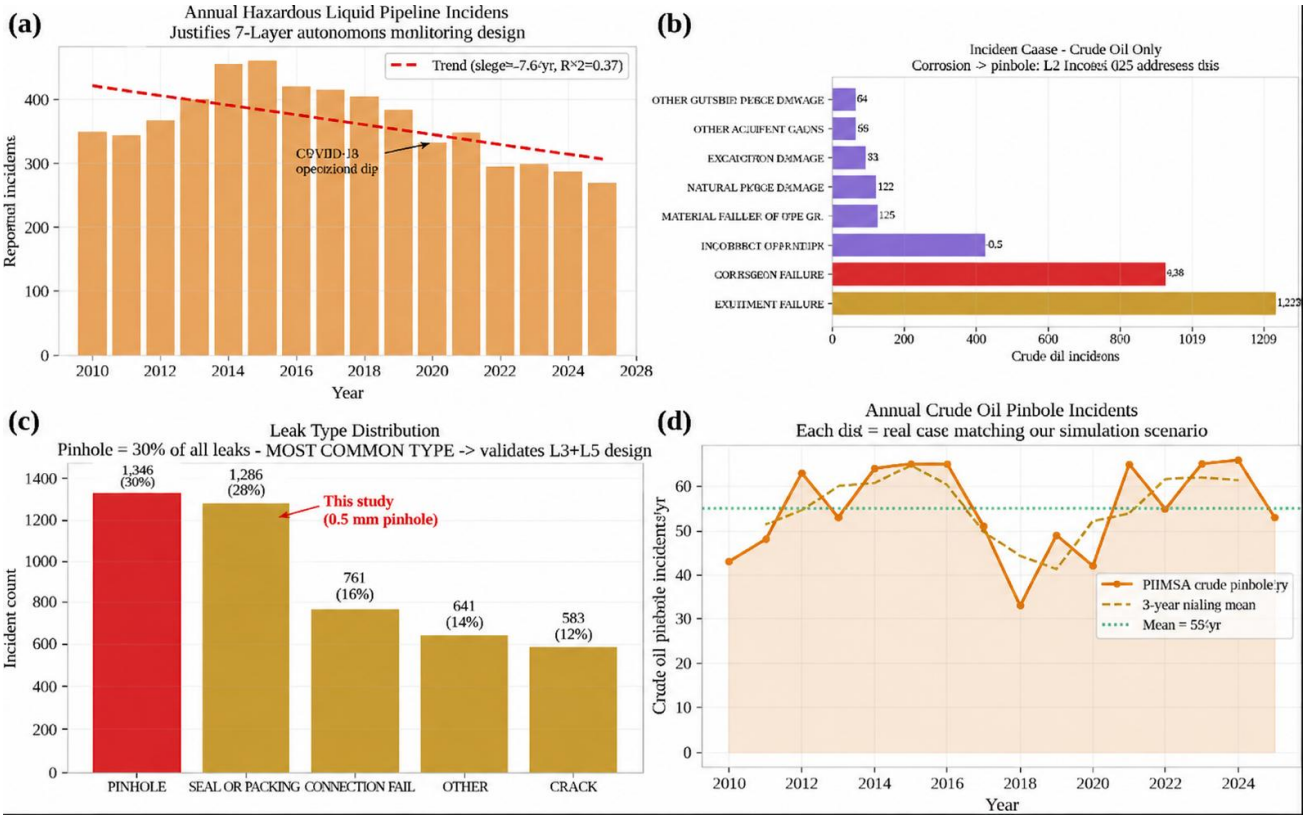

Fig 8: PHMSA incident data: (a) annual hazardous-liquid incidents with trend; (b) incident causes, crude oil only; (c) leak-type distribution; (d) annual crude-oil pinhole incidents.

Table 6 and Fig. 9 compare selected simulation parameters with PHMSA. The simulated operating pressure (1,813 psig) and pipe diameter (19.7 in) lie at the 99th and 80th PHMSA percentiles, so the simulated pipe lies inside the recorded envelope. The expected system survival of 89.49% is the product of the per-layer survival values assumed in the model (97.5% to 99.0%), not a measured quantity. Sensor fusion reduces the modelled detection time from over 24 h (the unaided pressure signal is below the noise) to under 30 s. For an equal 24 h window, healing reduces the modelled loss from 1,122 L to 3.89 L (Table 2 and Fig. 4(d)), a reduction of about 290 times. The 1.63 L figure in Table 6 is the ten-minute healed loss and is compared with the 24 h unhealed loss only for scale.

Table 6. Validation scorecard against PHMSA

Parameter	Simulation	PHMSA position
Pipe diameter	0.5 m (19.7 in)	P80
Operating pressure	125 bar (1,813 psi)	P99
Leak geometry	Pinhole	About 30%, most common
Unhealed loss, 24 h	1,122 L	P55
Healed loss, 10 min	1.63 L	P0 (simulation only)
Offshore pinholes	18 cases	30% of offshore total

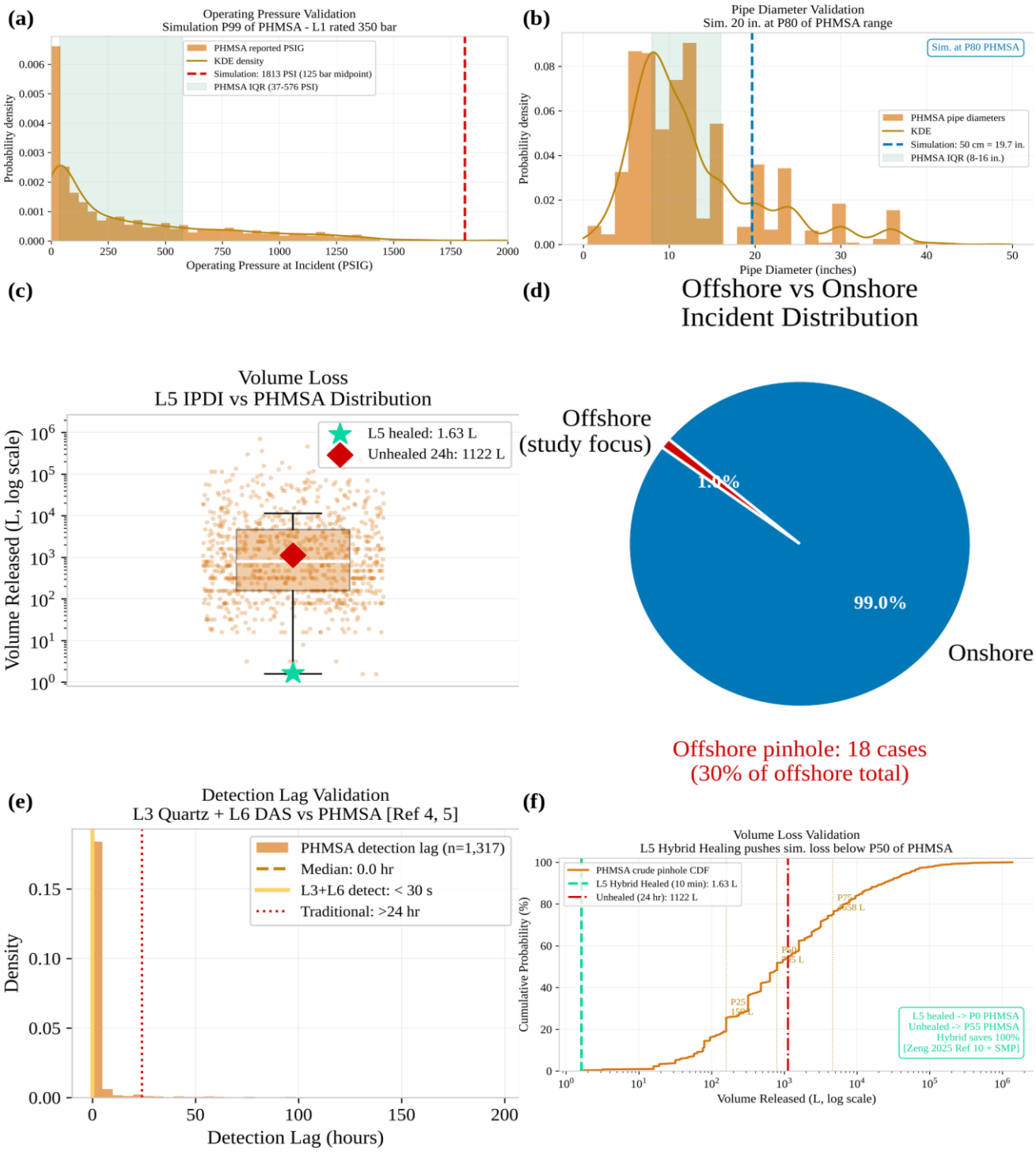

Fig 9: Comparison with PHMSA: (a) operating pressure; (b) pipe diameter; (c) volume released with simulated unhealed and healed values; (d) offshore versus onshore incidents; (e) detection lag; (f) cumulative distribution of volume released.

5.7 Random Forest sensor-fusion performance

Table 7 and Fig. 10 report the Random Forest results on the simulated sensor features. With 10-fold cross-validation, the classifier reaches an accuracy of 0.998 and an F1 score of 0.998, against 0.909 and 0.906 for the logistic-regression baseline. On the held-out set it misclassifies one of 200 cases (one false negative, no false positives). The AUC of 1.000 shows only that the simulated leak and no-leak classes are almost perfectly separable, since the training data come from the same physical model as the sensors. These figures must not be read as detection accuracy in the real world.

Table 7. Classifier performance on simulated data

Metric	RF 10-fold CV	LR 10-fold CV	RF held-out
Accuracy	0.998 ± 0.004	0.909 ± 0.035	0.995
Precision	1.000 ± 0.000	0.935 ± 0.046	1.000
Recall	0.996 ± 0.008	0.882 ± 0.053	0.990
F1 score	0.998 ± 0.004	0.906 ± 0.036	0.995
ROC AUC	1.000 ± 0.000	0.964 ± 0.017	1.000

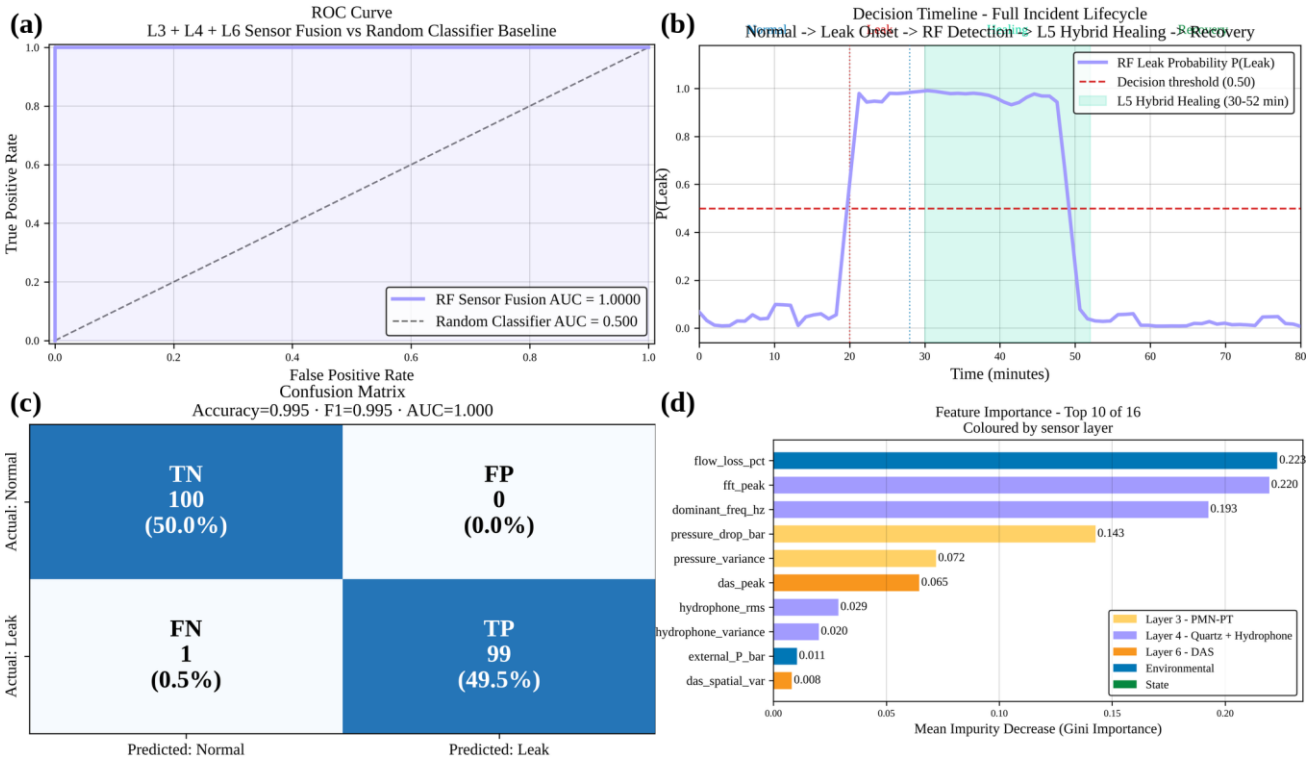

Fig 10: Random Forest sensor fusion: (a) ROC curve; (b) decision timeline over the incident lifecycle; (c) confusion matrix on the held-out set; (d) feature importance.

5.8 Comparative and economic discussion

Compared with a traditional coated pipeline with separate sensing, the proposed concept has a higher investment cost (about 5–6 times per metre) because of the fibre-optic communication, distributed sensing, power electronics and healing agent. In return it provides continuous multi-sensor sensing, self-repair of micro-cracks, communication redundancy and predictive maintenance. The economic case rests on savings from fewer unexpected repairs, faster detection and lower spill liability, which relate to the roughly 290-fold reduction in modelled 24 h oil loss described above. The cost ratio is an estimate and has not been verified against supplier data.

6. LIMITATIONS AND FUTURE WORK

The architecture has been evaluated only by simulation and has not been validated as a complete physical system. The scenario analysis uses the same physical model as the baseline, so it shows sensitivity rather than independent confirmation. The Random Forest is trained on synthetic data, and PHMSA data provide only historical context, not validation. Several model constants, such as the corrosion rates, per-layer survival values and radar scores, are assumptions. The healing efficiency is based on a coating tested at 150 bar, whereas the baseline external pressure is 302 bar. The L1 pressure rating also limits the design to about 3,480 m of depth.

Future work will cover: (i) pressure testing of L1 and L2 up to 350 bar; (ii) seawater ageing beyond the 1,008 h reported for IPDI@SPUA [37]; (iii) hydrophone and DAS calibration with a real leak; (iv) validation of the L7 power budget under real duty cycles; (v) improved leak localisation and rate estimation from real fused-sensor data; (vi) testing the classifier on data from other scenarios, such as other noise levels, leak sizes and multiple simultaneous leaks; and (vii) an operator dashboard and field-scale pilot deployment before any certification claim.

7. CONCLUSION

This paper introduced a seven-layer smart subsea pipeline that integrates environmental protection, structural strength, pressure/vibration monitoring, acoustic monitoring, hybrid self-healing, redundant fibre-optic communication and hybrid energy support. A physics-based simulation of a 50 km pipeline with a 0.5 m bore at 3,000 m depth gave a leak rate of about 0.01299 L/s for a 0.5 mm pinhole. Hybrid healing reduced the ten-minute cumulative leakage from 7.795 L to 1.629 L, a reduction of about 79.1%, and the reduction stayed between 65% and 81% across the healing-efficiency and timing scenarios tested. The 10-year power budget holds only at an average load below about 0.25 W, and the L1 pressure rating limits the design to about 3,480 m depth. Selected parameters lie inside the PHMSA envelope, and a simulated Random Forest fusion module separates the simulated classes almost perfectly. These results provide a basis for evaluating the concept, but experimental validation is still lacking.

Future work should move from simulation to hardware: hydrostatic and leak tests, healing-material ageing in seawater, sensor calibration against real leaks, and a field pilot. Extending the model to multiple leaks, higher-pressure designs and real sensor data would also strengthen the evidence.

8. ACKNOWLEDGMENTS

Data availability. The physics-based simulation code, the Random Forest implementation, the data-processing code and the figure-generation code are open source at https://github.com/Rajlohith/deep-sea-pipeline-pinhole-leak-and-self-healing-simulation. The PHMSA hazardous-liquid data are available from the PHMSA website [1].

9. REFERENCES

[1] Pipeline and Hazardous Materials Safety Administration, “Pipeline incident data and hazardous liquid accident statistics,” U.S. Department of Transportation. [Online].

Available: https://www.phmsa.dot.gov/data-and-statistics/pipeline/distribution-transmission-gathering-lng-and-liquid-accident-and-incident-data

[2] H. Fan, S. Tariq, and T. Zayed, "Acoustic leak detection approaches for water pipelines," Autom. Constr., vol. 138, Art. no. 104226, 2022, doi: 10.1016/j.autcon.2022.104226.

[3] G. M. Wenz, "Acoustic ambient noise in the ocean: Spectra and sources," J. Acoust. Soc. Amer., vol. 34, no. 12, pp. 1936–1956, 1962, doi: 10.1121/1.1909155.

[4] J. M. López-Higuera, L. R. Cobo, A. Q. Incera, and A. Cobo, "Fiber optic sensors in structural health monitoring," J. Lightw. Technol., vol. 29, no. 4, pp. 587–608, 2011, doi: 10.1109/JLT.2011.2106479.

[5] A. Xenaki, P. Gerstoft, E. Williams, and S. Abadi, "Overview of distributed acoustic sensing: Theory and ocean applications," J. Acoust. Soc. Amer., vol. 158, no. 1, pp. 801–825, 2025, doi: 10.1121/10.0037218.

[6] S. R. White et al., "Autonomic healing of polymer composites," Nature, vol. 409, pp. 794–797, 2001, doi: 10.1038/35057232.

[7] K. S. Toohey, N. R. Sottos, J. A. Lewis, J. S. Moore, and S. R. White, "Self-healing materials with microvascular networks," Nat. Mater., vol. 6, pp. 581–585, 2007, doi: 10.1038/nmat1934.

[8] E. Koştur, N. Geren, and M. Özkutlu Demirel, "Novel microvascular channel method for developing self-healing functions of composite structures," Compos. Part A: Appl. Sci. Manuf., vol. 199, Art. no. 109226, 2025, doi: 10.1016/j.compositesa.2025.109226.

[9] S. R. M. Paladugu et al., "A comprehensive review of self-healing polymer, metal, and ceramic matrix composites and their modeling aspects for aerospace applications," Materials, vol. 15, no. 23, Art. no. 8521, 2022, doi: 10.3390/ma15238521.

[10] S. Islam and G. Bhat, "Progress and challenges in self-healing composite materials," Mater. Adv., vol. 2, no. 6, pp. 1896–1926, 2021, doi: 10.1039/D0MA00873G.

[11] C. Rodrigues et al., "Emerging triboelectric nanogenerators for ocean wave energy harvesting: State of the art and future perspectives," Energy Environ. Sci., vol. 13, pp. 2657–2683, 2020, doi: 10.1039/D0EE01258K.

[12] M. Salman, V. Sorokin, and K. Aw, "Systematic literature review of wave energy harvesting using triboelectric nanogenerator," Renew. Sustain. Energy Rev., vol. 201, Art. no. 114626, 2024, doi: 10.1016/j.rser.2024.114626.

[13] G. Li and W. Zhu, "Tidal current energy harvesting technologies: A review of current status and life cycle assessment," Renew. Sustain. Energy Rev., vol. 179, Art. no. 113269, 2023, doi: 10.1016/j.rser.2023.113269.

[14] M. J. Khan, G. Bhuyan, M. T. Iqbal, and J. E. Quaicoe, "Hydrokinetic energy conversion systems and assessment of horizontal and vertical axis turbines for river and tidal applications," Appl. Energy, vol. 86, no. 10, pp. 1823–1835, 2009, doi: 10.1016/j.apenergy.2009.02.017.

[15] Y. Ma, L. Cui, H. Zhou, and S. Bhattacharya, "Hybrid offshore renewable energy harvest system: A review," Energy Convers. Manage., vol. 348, Part A, Art. no. 120654, 2026, doi: 10.1016/j.enconman.2025.120654.

[16] J. Liu, B. Bao, J. Chen, Y. Wu, and Q. Wang, "Marine energy harvesting from tidal currents and offshore winds: A 2-DOF system based on flow-induced vibrations," Nano Energy, vol. 114, Art. no. 108664, 2023, doi: 10.1016/j.nanoen.2023.108664.

[17] X. Lu et al., "Superior toughness–strength epoxy via biocomposite curing for deep-sea equipment using multifunctional syntactic foams," ACS Appl. Polym. Mater., vol. 7, no. 19, pp. 13296–13309, 2025, doi: 10.1021/acsapm.5c02794.

[18] S. Anirudh, C. G. Jayalakshmi, A. Anand, B. Kandasubramanian, and S. O. Ismail, "Epoxy/hollow glass microsphere syntactic foams for structural and functional application—A review," Eur. Polym. J., vol. 171, Art. no. 111163, 2022, doi: 10.1016/j.eurpolymj.2022.111163.

[19] G. Loubrieu et al., "Hydrostatic strength of hollow glass microspheres composites: Influencing factors and modelling," Compos. Part C: Open Access, vol. 8, Art. no. 100286, 2022, doi: 10.1016/j.jcomc.2022.100286.

[20] M. J. A. Smith, Z. Yousaf, P. Potluri, and W. J. Parnell, "Modelling hollow thermoplastic syntactic foams under high-strain compressive loading," Compos. Sci. Technol., vol. 213, Art. no. 108882, 2021, doi: 10.1016/j.compscitech.2021.108882.

[21] Z. Yousaf, N. F. Morrison, and W. J. Parnell, "Tensile properties of all-polymeric syntactic foam composites: Experimental characterization and mathematical modelling," Compos. Part B: Eng., vol. 231, Art. no. 109556, 2022, doi: 10.1016/j.compositesb.2021.109556.

[22] S. Selcuk, U. Ahmetoglu, and E. C. Gokce, "Basalt fiber reinforced polymer composites (BFRP) other than rebars: A review," Mater. Today Commun., vol. 37, Art. no. 107359, 2023, doi: 10.1016/j.mtcomm.2023.107359.

[23] V. Fiore, T. Scalici, G. Di Bella, and A. Valenza, "A review on basalt fibre and its composites," Compos. Part B: Eng., vol. 74, pp. 74–94, 2015, doi: 10.1016/j.compositesb.2014.12.034.

[24] X. Deng, M. S. Hoo, Y. W. Cheah, and L. Q. N. Tran, "Processing and mechanical properties of basalt fibre-reinforced thermoplastic composites," Polymers, vol. 14, no. 6, Art. no. 1220, 2022, doi: 10.3390/polym14061220.

[25] L. Huang, S. Gong, G. Li, S. Li, K. Tang, and W. Wang, "Mechanical properties and tensile intrinsic study of basalt fibre-silicon carbide (SiC) co-reinforced polyurethane cement mortar," Mater. Des., vol. 261, Art. no. 115299, 2026, doi: 10.1016/j.matdes.2025.115299.

[26] Special Metals Corporation, "INCONEL alloy 625," Technical Bulletin, 2013. [Online]. Available: https://www.specialmetals.com/documents/technical-bulletins/inconel/inconel-alloy-625.pdf

[27] S. Zhang, F. Li, J. Luo, R. Sahul, and T. R. Shrout, "Relaxor-PbTiO3 single crystals for various applications," IEEE Trans. Ultrason., Ferroelectr., Freq. Control, vol. 60, no. 8, pp. 1572–1580, 2013, doi: 10.1109/TUFFC.2013.2737.

[28] J. Tian and P. Han, "Growth and characterization on PMN-PT-based single crystals," Crystals, vol. 4, no. 3, pp. 331–341, 2014, doi: 10.3390/cryst4030331.

[29] M. Ju, Z. Dou, J.-W. Li, X. Qiu, B. Shen, D. Zhang, F.-Z. Yao, W. Gong, and K. Wang, "Piezoelectric materials and sensors for structural health monitoring: Fundamental aspects, current status, and future perspectives," Sensors, vol. 23, no. 1, Art. no. 543, 2023, doi: 10.3390/s23010543.

[30] B. Abdul, V. M. Mastronardi, A. Qualtieri, L. Algieri, F. Guido, F. Rizzi, and M. De Vittorio, "Sensitivity and directivity analysis of piezoelectric ultrasonic cantilever-based MEMS hydrophone for underwater applications," J. Mar. Sci. Eng., vol. 8, no. 10, Art. no. 784, 2020, doi: 10.3390/jmse8100784.

[31] S. Shi, W. Geng, K. Bi, J. He, X. Hou, J. Mu, F. Li, and X. Chou, "Design and fabrication of a novel MEMS piezoelectric hydrophone," Sens. Actuators A: Phys., vol. 313, Art. no. 112203, 2020, doi: 10.1016/j.sna.2020.112203.

[32] S. Choi, H. Lee, and W. Moon, "A micro-machined piezoelectric hydrophone with hydrostatically balanced air backing," Sens. Actuators A: Phys., vol. 158, pp. 60–71, 2010, doi: 10.1016/j.sna.2009.12.019.

[33] W. Wang, Y. Pei, L. Ye, and K. Song, "High-sensitivity cuboid interferometric fiber-optic hydrophone based on planar rectangular film sensing," Sensors, vol. 20, no. 22, Art. no. 6422, 2020, doi: 10.3390/s20226422.

[34] B. Bakhtawar and T. Zayed, "Review of water leak detection and localization methods through hydrophone technology," J. Pipeline Syst. Eng. Pract., vol. 12, no. 4, Art. no. 03121002, 2021, doi: 10.1061/(ASCE)PS.1949-1204.0000574.

[35] M. M. Adil, M. S. Rabbi, and T. Tasnim, "Development of microcapsule-based self-healing composite: A critical review on influencing factors of microencapsulation, healing efficiency, thermal stability and application," Alexandria Eng. J., vol. 122, pp. 1–17, 2025, doi: 10.1016/j.aej.2025.02.092.

[36] N. J. Kanu, E. Gupta, U. K. Vates, and G. K. Singh, "Self-healing composites: A state-of-the-art review," Compos. Part A: Appl. Sci. Manuf., vol. 121, pp. 474–486, 2019, doi: 10.1016/j.compositesa.2019.04.012.

[37] X. Zeng et al., "Self-healing performance and anticorrosion mechanism of microcapsule-containing epoxy coatings under deep-sea environment," Prog. Org. Coat., vol. 203, Art. no. 109176, 2025, doi: 10.1016/j.porgcoat.2025.109176.

[38] X. Liang, S. Liu, H. Yang, and T. Jiang, "Triboelectric nanogenerators for ocean wave energy harvesting: Unit integration and network construction," Electronics, vol. 12, no. 1, Art. no. 225, 2023, doi: 10.3390/electronics12010225.

[39] P. Simon and Y. Gogotsi, "Materials for electrochemical capacitors," Nat. Mater., vol. 7, pp. 845–854, 2008, doi: 10.1038/nmat2297.

[40] L. Breiman, "Random forests," Mach. Learn., vol. 45, no. 1, pp. 5–32, 2001, doi: 10.1023/A:1010933404324.

[41] F. Pedregosa et al., "Scikit-learn: Machine learning in Python," J. Mach. Learn. Res., vol. 12, pp. 2825–2830, 2011. [Online]. Available: https://www.jmlr.org/papers/v12/pedregosa11a.html